Causes of Reduced Climate Sensitivity in E3SM from Version 1 to Version 2

Yi Qin[1,2], Xue Zheng[1], Stephen A. Klein[1], Mark D. Zelinka[1], Po-Lun Ma[2], Jean-Christophe Golaz[1], Shaocheng Xie[1]

[1] Lawrence Livermore National Laboratory, Livermore, CA, USA.

[2] Pacific Northwest National Laboratory, Richland, WA, USA.

Corresponding author: Yi Qin (yi.qin@pnnl.gov)

Key Points:

- E3SM's effective climate sensitivity is lower in version 2 mainly due to the reduced positive cloud feedback over marine low cloud regions
- The feedback reduction is primarily due to altered cloud microphysical parameters and a new deep convection trigger function
- Process-level analysis is conducted to understand the impact of these model modifications on cloud feedbacks.

Abstract

The effective climate sensitivity in the Department of Energy's Energy Exascale Earth System Model (E3SM) has decreased from 5.3 K in version 1 to 4.0 K in version 2. This reduction is mainly due to a weaker positive cloud feedback that leads to a stronger negative radiative feedback. Present-day atmosphere-only experiments with uniform 4 K sea surface temperature warming are used to separate the contributions of individual model modifications to the reduced cloud feedback. We find that the reduced cloud feedback is mostly driven by changes over the tropical marine low cloud regime, mainly related to a new trigger function for the deep convection scheme and modifications in the cloud microphysics scheme. The new trigger function helps weaken the low cloud reduction by increasing the cloud water detrainment at low levels from deep convection under warming. Changes to the formula of autoconversion rate from liquid to rain and an introduced minimum cloud droplet number concentration threshold in cloud microphysical calculations help sustain clouds against dissipation by suppressing precipitation generation with warming. In the midlatitudes, the increased Wegener-Bergeron-Findeisen (WBF) efficiency strongly reduces present-day liquid water and leads to a stronger negative cloud optical depth feedback. The reduced trade cumulus cloud feedback in v2 is closer to estimates from recent observational and large-eddy modeling studies but might not be due to the right physical reasons. The reduced mid-latitude cloud feedback may be more plausible because more realistic present-day mixed-phase clouds are produced through the change in the WBF efficiency.

Plain Language Summary

Understanding how the Earth responds to greenhouse gas increases is important for climate change research. In the Department of Energy's Energy Exascale Earth System Model, the global temperature response to an abrupt quadrupling of atmospheric carbon dioxide has decreased from 5.3 K in version 1 to 4.0 K in version 2. This reduction is mainly because low-level clouds over the tropical oceans decrease less as the planet warms in version 2: a weaker amplifying cloud feedback. To understand the reasons behind this reduction, warming simulations were conducted to separate the contributions of individual model changes. We find that the reduced cloud feedback is primarily due to changes in the representation of the vertical movement of air through the depth of the lower atmosphere and of the microscopic properties of

clouds. The findings highlight some unexpected impacts on cloud feedback resulting from modifications to the model's physics and emphasize the importance of monitoring and understanding changes in cloud feedback during model development.

1 Introduction

Equilibrium climate sensitivity (ECS), the global mean surface air temperature response (ΔT) to doubling atmospheric carbon dioxide concentration, is an important measure of climate change but has large uncertainties. Effective climate sensitivity (EffCS) is closely related to ECS, and represents the ΔT in response to doubling carbon dioxide concentration assuming a time-invariant radiative feedback parameter. The Coupled Model Intercomparison Project Phase 6 (CMIP6) models exhibit a larger multi-model average and inter-model spread in EffCS compared to CMIP5 models (M. D. Zelinka et al., 2020). In particular, 23 out of 53 models have EffCS greater than 4 K (M. Zelinka, 2022), the upper bound of the likely ECS range as determined by the sixth Assessment Report of the Intergovernmental Panel on Climate Change (IPCC) (Forster et al., 2021). Zelinka et al. (2020) indicated that the large spread of the cloud feedback is the main contributor to the broader EffCS range and higher average EffCS in CMIP6. Therefore, understanding the cloud feedback in each model is crucial for understanding the uncertainties of EffCS.

Version one of the Department of Energy's Energy Exascale Earth System Model (E3SMv1), with an EffCS of 5.3 K, is one of the CMIP6 models lying above the IPCC likely range. This is mainly because of its strong positive cloud feedback (J. Golaz et al., 2019; M. D. Zelinka et al., 2022). The recently released E3SM version 2 (E3SMv2) shows a reduced EffCS (4.0 K) with improved mean-state clouds and precipitation (J. Golaz et al., 2022). Here, we conduct targeted experiments with the two versions of E3SM to establish what leads to the reduced EffCS in E3SMv2 and whether it is related to the improved process-level representation, as has been done in previous studies (Bodas-Salcedo et al., 2019; Gettelman et al., 2012, 2019; Webb et al., 2006). We will describe and analyze the reasons for E3SM’s reduced EffCS, especially its reduced cloud feedbacks, and their relationship to modifications of physical parameterizations from E3SMv1 to E3SMv2.

The paper is organized as follows. Section 2 describes the model, experimental setup, and diagnostic methods. Atmosphere-only experiments with uniform 4 K sea surface temperature (SST) warming have been shown to provide a good estimate of the cloud feedback in the fully coupled experiment (Qin et al., 2022; Ringer et al., 2014), and are mainly used to diagnose the impacts of model modifications on the cloud feedback changes. In Section 3, we first investigate the reasons for the reduced EffCS by examining the individual radiative feedbacks and forcings, demonstrating the dominant role of cloud feedback change. Next, we revert parameterization settings or configurations in E3SMv2 to those used in E3SMv1 to identify the impact of individual modifications on the present-day mean climate and its response to warming. In Section 4, we explore the physical processes that explain how the individual model modifications affect the cloud feedback and its evolution from E3SMv1 to E3SMv2. We summarize our main findings and provide further discussion in Section 5.

2 Methods

2.1 Model and simulations

E3SM is a state-of-the-art climate model, which includes atmosphere, land, ocean, sea ice and river routing components. Its version 1 (E3SMv1) (J. Golaz et al., 2019) has an EffCS of 5.3 K. Its version 2 (E3SMv2) has a lower EffCS (4.0 K) with improved present-day climate in simulated clouds and precipitation. Specific improvements include a reduced double ITCZ bias, reduced dry Amazon bias, and improved stratocumulus clouds, among others. Detailed comparison between these two versions was documented in Golaz et al. (2022).

To understand the reduced cloud feedback of E3SMv2, we constructed a series of "intermediate" versions by taking E3SMv2 and reverting individual modifications that were made in going from E3SMv1 to E3SMv2. We start from E3SMv2 and revert pieces instead of implementing modifications in E3SMv1 because E3SMv2 is computationally nearly twice as fast as E3SMv1, facilitating the sensitivity experiments listed below. All major atmospheric physics modifications from E3SMv1 to E3SMv2 are first organized at the physical parameterization level, following Ma et al. (2022): Cloud Layers Unified By Binormals (CLUBB) (J.-C. Golaz et al., 2002; Larson, 2017), cloud microphysics (MG) (Gettelman & Morrison, 2015; Morrison & Gettelman, 2008), Zhang-McFarlane deep convection (ZM) (G. J. Zhang & McFarlane, 1995), surface wind gustiness (gust) affecting the calculation of surface fluxes(Harrop et al., 2018; Ma

et al., 2022; Redelsperger et al., 2000), gravity wave (gw) (Richter et al., 2019), and others including tuning factors related to sea salt, dust, ozone and the ice nucleation SO_2 size threshold for the Aitken mode.

A brief description of the major parameterization changes between E3SMv1 and E3SMv2 helps to understand differences seen below. Parameters in CLUBB and MG were modified to better represent transitions between stratocumulus and trade cumulus clouds and represent precipitation in subtropical marine low cloud regions (Ma et al., 2022). The scaling factor of the Wegener-Bergeron-Findeisen (WBF) process is increased in E3SMv2 for ice and mixed-phase clouds, enhancing ice crystal growth at the expense of liquid droplets, and reducing an apparent over-prediction of supercooled liquid found in E3SMv1. The modifications in ZM include a new trigger function (Xie et al., 2019) based on dynamic Convective Available Potential Energy (dCAPE) (Xie & Zhang, 2000) with an Unrestricted air parcel Launch Level (ULL) (Wang et al., 2015) which replaces the original CAPE trigger function. Other ZM parameters were re-tuned, such as the autoconversion coefficient for convective clouds. The new trigger function reduces the occurrence of deep convection over most regions and improves the precipitation simulation, particularly the diurnal cycle (Xie et al., 2019). More details about the tuning strategy and their impacts on the present-day simulation can be found in Golaz et al. (2022) and Ma et al. (2022).

For those dominant physical parameterizations (i.e., ZM and MG), we further conducted subgroup experiments to isolate the impact of individual modifications. We separate modifications in ZM into two groups: trigger function (ZMtrig) and other modifications except for the trigger function (ZMother). In addition, the impact of the changes to each tuning parameter in MG is evaluated separately. All grouped and subgrouped modifications are summarized in Table 1 and further discussed below.

Table 1. Modifications from E3SMv1 to E3SMv2.

	Description	**v1**	**v2**	**Subgroups**
CLUBB (clubb)				
clubb_c14	Coefficient for $\overline{u'^2}$ and $\overline{v'^2}$ damping	1.06	2.5	

clubb_c_k10	Ratio of eddy diffusivity of momentum to eddy diffusivity of scalars	0.3	0.35	
clubb_c_k10h	Ratio of eddy diffusivity of thermodynamic variables to eddy diffusivity of scalars	0.3	0.35	
clubb_wpxp_l_thresh	Eddy length scale threshold for Newtonian and buoyancy damping of $\overline{w'q_t'}$ and $\overline{w'\theta_l'}$ (m)	60	100	
clubb_c1	Coefficient for $\overline{w'^2}$ damping at low Sk_w	1.335	2.4	
clubb_c1b	Coefficient for $\overline{w'^2}$ damping at high Sk_w	1.335	2.8	
clubb_c1c	Coefficient for Sk_w dependency of clubb_c1	1	0.75	
clubb_c6rtb	Coefficient for water flux ($\overline{w'q_t'}$) damping at high Sk_w	6	7.5	
clubb_c6thlb	Coefficient for temperature flux ($\overline{w'\theta_l'}$) damping at high Sk_w	6	7.5	
clubb_c6rtc	Coefficient for Sk_w dependency of clubb_c6rt	1.0	0.5	
clubb_c6thlc	Coefficient for Sk_w dependency of clubb_c6thl	1.0	0.5	
clubb_c11	Coefficient for $\overline{w'^3}$ damping at low Sk_w	0.8	0.7	
clubb_c11b	Coefficient for $\overline{w'^3}$ damping at high Sk_w	0.35	0.2	
clubb_c11c	Coefficient for Sk_w dependency of clubb_c11	0.5	0.85	
clubb_gamma_coef	The width of the Gaussian distribution at low Sk_w	0.32	0.12	
clubb_gamma_coefb	The width of the Gaussian distribution at high Sk_w	0.32	0.28	
clubb_gamma_coefc	Coefficient for Sk_w dependency of the Gaussian distribution width	N/A	1.2	
clubb_c8	Coefficient for $\overline{w'^3}$ damping	4.3	5.2	
clubb_mu	Fractional parcel entrainment rate per unit height (1/m)	1.0E-03	5.0E-4	
clubb_ice_deep	Assumed ice condensate radius detrained from ZM (m)	1.6E-05	1.4E-5	
clubb_ipdf_call_placement	Select the placement of the call to CLUBB's PDF: 1) Call before advancing predictive fields; 2) Call after advancing predictive fields; 3) Call both before and after advancing predictive fields	1	2	
Microphysics (MG)				
micro_mg_berg_eff_factor	Efficiency factor for the Wegener-Bergeron-Findeisen (WBF) process	0.1	0.7	MG_WBF
micro_mincdnc	Minimum droplet number conc (#/m^3) imposed when micro_mincdnc > 0	N/A	10.E6	MG_mincdnc

microp_aero_wsubmin	Minimum subgrid vertical velocity for liquid droplet nucleation (m/s)	0.2	0.1	MG_wsub
micro_mg_accre_enhan_fac	Coefficient for liquid cloud accretion rate formula	1.5	1.75	MG_accre
prc_exp1	Exponent of liquid droplet number concentration in autoconversion rate formula	-1.2	-1.4	MG_auto
ZM deep convection except trigger function (ZMother)				
zmconv_alfa	Downdraft mass flux fraction adjustment	0.1	0.14	
zmconv_c0_lnd	Autoconversion coefficient over land in ZM	0.007	0.002	
zmconv_c0_ocn	Autoconversion coefficient over ocean in ZM	0.007	0.002	
zmconv_mx_bot_1yr_adj	Number of lowest layers skipped for computing maximum moist static energy	2	1	
zmconv_tp_fac	Temperature perturbation scale factor	0	2	
cldfrc_dp1	Parameter for deep convection cloud fraction	0.045	0.018	
Trigger (ZMtrig)				
zmconv_trigdcape_ull	Use of dCAPE trigger along with ULL	.false.	.true.	
Gravity wave (gw)				
effgw_beres	Efficiency associated with convective gravity waves from the Beres scheme (Beres et al., 2004)	0.4	0.35	
effgw_oro	Efficiency associated with orographic gravity waves	0.25	0.375	
gw_convect_hcf	Heating rate conversion factor associated with convective gravity waves	20	10	
Gustiness (gust)				
clubb_use_sgv	Enable subgrid wind and temperature variances in the surface flux	.false.	.true.	
Others				
seasalt_emis_scale	Sea salt aerosol emission tuning factor	0.85	0.6	
dust_emis_fact	Tuning parameter for dust emissions	2.05	1.5	
linoz_psc_t	Tunable Linoz PSC ozone loss temperature (K) threshold	193	197.5	
so4_sz_thresh_icenuc	Aitken mode sulfate aerosol size threshold for homogeneous ice nucleation (m)	5.0E-8	8.0E-8	

We use fixed SST experiments (Hansen et al., 2005) to investigate the impact of modifications on feedback changes between E3SMv1 and E3SMv2. The control experiment (CTL) is an atmosphere-only experiment with prescribed observed climatological (2005-2014)

monthly sea surface temperature (SST) and forcing agents. The warming experiment (P4K) is conducted by prescribing a uniform SST 4 K warming to the control experiment. For all sensitivity experiments, control and warming simulations are run for 6 years and the last 5 years are used in the analysis. Note that all simulations were not re-tuned to get a good top of the atmosphere balance.

2.2 Analysis method

For the coupled experiments of E3SMv1 and E3SMv2, the radiative feedback and effective radiative forcing are computed by regressing annual mean top-of-atmosphere (TOA) net radiation anomalies onto global- and annual-mean surface air temperature anomalies (ΔT_s) over the 150-year abrupt-4xCO2 experiments. Anomalies are computed with respect to the contemporaneous piControl experiments. The radiative feedback is the regression slope and the effective radiative forcing is the y intercept divided by 2 (Gregory et al., 2004). For the atmosphere-only experiments of both E3SMv1 and E3SMv2 and the sensitivity experiments, the radiative feedback is computed as the global TOA net radiation anomaly divided by the global-mean T_s anomaly, where the anomalies are computed as the differences between P4K and CTL climatologies.

We estimate radiative feedbacks using radiative kernels, which quantify the impact on TOA radiation from small changes in climate fields ($\partial R/\partial x_i$ where x_i includes surface and atmospheric temperature, water vapor, and surface albedo). These are multiplied by component changes mediated by the global- and annual-mean surface temperature (dx_i/dT_s). In Figure 1, we show the feedbacks decomposed into components advocated by Held & Shell (2012): the Planck and lapse rate feedbacks at constant relative humidity, the feedback from changes in relative humidity, the surface albedo feedback, and the cloud feedback. The cloud feedback is computed by adjusting the temperature-mediated change in cloud radiative effect for cloud masking effects (Shell et al., 2008; Soden et al., 2008). The small residual term is due to the assumptions and approximations in the radiative kernel method. Additionally, we also estimate the cloud feedback due to cloud amount, altitude and optical depth changes using cloud radiative kernels and ISCCP simulator cloud output (Zelinka et al., 2012, 2016).

To better understand which regimes lead to the cloud feedback reduction from E3SMv1 to E3SMv2, we average results within five regimes. Regimes are first defined by latitude bands

outside of the tropics: 90°–60°S and 60°–90°N are combined as 'HiLat' regime and 60°–30°S and 60°–30°N are combined as 'MidLat' regime. The Tropics (30°S-30°N) are divided into three regimes based on land and ocean and climatological vertical velocity at 700 hPa (ω_{700}) averaged between the CTL and P4K experiments: tropical marine low cloud (TropMarineLow; ocean, $\omega_{700} > 0$ hPa/day), tropical marine ascent (TropAscent; ocean, $\omega_{700} < 0$ hPa/day) and tropical land (TropLand) regimes. Figure S1 shows the spatial coverage of five cloud regimes in E3SMv2. The fractional areas of tropical marine low cloud and tropical ascent regimes differ less than 1% in all experiments (not shown). Note that the results are qualitatively similar if we use only ω_{700} from CTL or P4K experiments or we use ensemble mean ω_{700} from all experiments.

3 Overall evaluation

3.1 Radiative feedbacks and forcing from 4xCO2

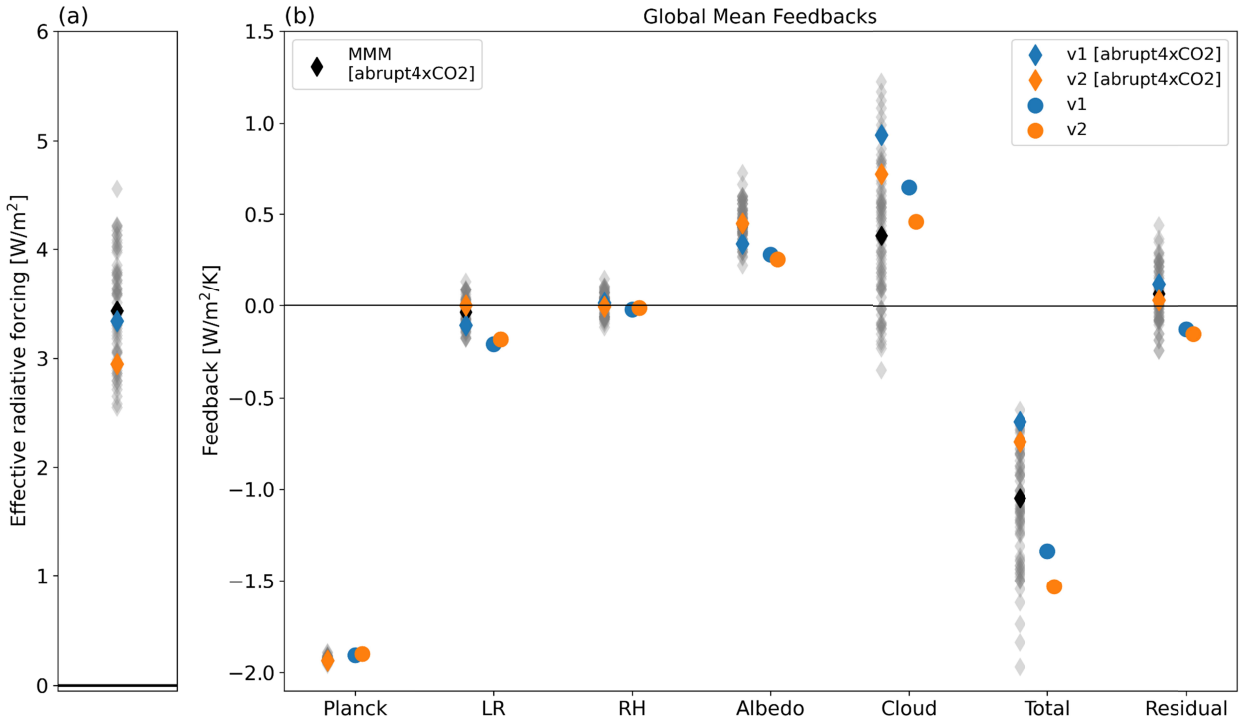

Figure 1. Global-mean (a) $4xCO_2$ effective radiative forcing (ERF) (W/m^2) and (b) radiative feedbacks (W/m^2/K) from the 150 yr coupled E3SMv1 (v1 [abrupt-4xCO2]), the 150 yr coupled E3SMv2 (v2 [abrupt-4xCO2]), the 5 yr atmosphere-only E3SMv1 (v1) and the 5 yr atmosphere-only E3SMv2 (v2). ERFs and feedbacks from other CMIP5 and CMIP6 models are labeled as gray diamonds with the multi-model mean (MMM) value labeled as the black bold diamond. The

residual term is the difference between the total radiative feedback and the sum of kernel derived components. ERFs are derived using the full 150 yr coupled experiments.

Because the reduced EffCS of E3SMv2 relative to E3SMv1 could be the result of changes in effective radiative forcing (ERF) or changes in radiative feedback, we first compare the 4xCO_2 ERF and feedbacks between E3SMv1 and E3SMv2 in both coupled and atmosphere-only experiments (Figure 1). In 150 yr abrupt-4xCO2 experiments, ERF in E3SMv2 is 12% smaller than that in E3SMv1 (2.95 vs 3.34 W/m^2), and the total radiative feedback is 17% larger in magnitude than that in E3SMv1 (-0.74 vs -0.63 W/m^2/K). To determine the relative importance of changes in ERF from changes in feedback in driving reduced EffCS in v2, we follow the procedure described in Zelinka et al (2020). Briefly, we estimate the impact on EffCS from the v1-to-v2 change in ERF holding the feedback fixed at its v1 value, and the impact on EffCS from the change in feedback holding ERF fixed at its v1 value. Unlike in Zelinka et al (2020), we do this calculation using ERF values derived from amip-4xCO2 simulations and feedback values derived from amip-p4K simulations (Table S1). Doing so ensures that ERF and feedback are derived independently, which is not the case when both are estimated as the regression slope and intercept from the abrupt-4xCO2 experiment. These ERF and feedback values closely capture the EffCS change seen in the coupled experiments, and we find that the feedback reduction contributes 82% to the reduced EffCS from E3SMv1 to E3SMv2, with the ERF reduction contributing the remaining 18%. Therefore, the reduced EffCS in v2 is largely caused by the reduced feedback, and we will focus on the feedback change in the remaining analyses.

The more negative total feedback in E3SMv2 mainly results from the weakened total cloud feedback (0.72 vs 0.93 W/m^2/K) with partial compensation from increased albedo and lapse rate feedbacks. The atmosphere-only experiments largely reproduce the total cloud feedback reduction from E3SMv1 to E3SMv2 – a reduction of 0.19 W/m^2/K for the atmosphere-only experiment vs 0.21 W/m^2/K for coupled experiment – although they underestimate the coupled total cloud feedback for both E3SMv1 and E3SMv2. This underestimate can be alleviated by prescribing an SST warming pattern derived from the corresponding 150yr fully-coupled experiment to the atmosphere-only experiment rather than using the spatially uniform 4K warming (not shown).

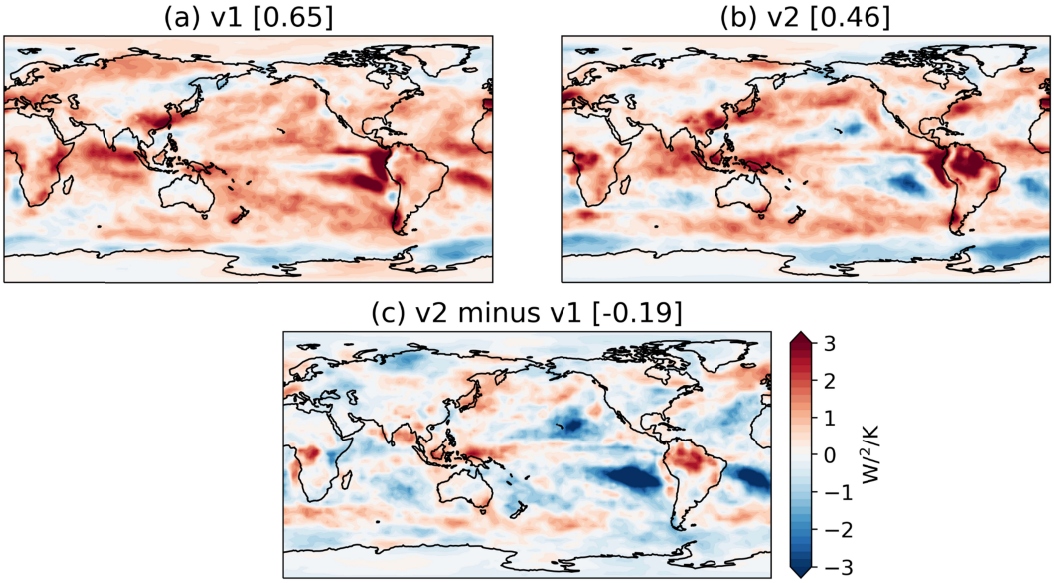

Figure 2. Spatial distribution of total cloud feedbacks from atmosphere-only (a) v1, (b) v2 and (c) the difference between v2 and v1. Global mean values are labeled in each bracket.

The spatial distribution of cloud feedbacks for atmosphere-only and coupled experiments is presented in Figure 2 and Figure S2, respectively. From the global mean to the spatial distribution, atmosphere-only experiments with uniform 4 K SST warming well capture the reduced global-mean net cloud feedback (mainly caused by low clouds) and can also capture the dominant regions with pronounced reduction of cloud feedback from E3SMv1 to E3SMv2.

3.2 Attribution of cloud feedback change to specific parameterization modifications

In this section, we investigate the impact of individual modifications from E3SMv1 to E3SMv2 on the cloud feedback using a set of atmosphere-only experiments listed in Section 2. The naming convention for the simulations hereafter indicates the base model (v2) followed in parentheses by the relevant parameterization or configuration grouping that has been reverted back to v1 settings. We first conduct a simulation called 'v2.v1(All)', which is based on v2 with all major physical modifications reverted to their v1 settings (Table 2) to ensure that the main contributors to the cloud feedback reduction are captured. The global mean total cloud feedback is 0.61 W/m^2/K in v2.v1(All), quite close to that in v1 (0.65 W/m^2/K). The difference of the total cloud feedback between v2 and v2.v1(All) is also quite similar to that difference between v2 and

v1 (Figure S3) with a spatial correlation of 0.80. Results for v2.v1(All) are not identical to those of v1 because v2.v1(All) does not include the modifications related to dynamics, such as the new dynamical core, semi-Lagrangian tracer transport, and physics grid (Golaz et al., 2022), which lack a direct physical connection to the cloud feedback changes. In the tropical marine low cloud regime (Figure 3), the difference between v2.v1(All) and v1 appears to be non-negligible and comparable to the difference of other modifications. For this regime, further understanding of the impact of other non-physical related modifications would be useful. Considering the good correspondence between v2.v1(All) and v1, we therefore conclude that v2.v1(All) includes the main modifications contributing to the cloud feedback reduction from v1 to v2. We will focus on the difference between v2 and v2.v1(All) in subsequent analyses.

Table 2. Description of progressively reverted simulations from v2 to v1. In the description, the bold italicized text denotes the base experiment and the non-italicized text denotes the added configuration relative to the base experiment.

Short Name	Description
v2	E3SMv2
v2.v1(clubb)	***v2*** +CLUBB related parameters changed from the settings in v2 to those of v1
v2.v1(clubb.MG)	***v2.v1(clubb)*** + MG related parameters changed from the settings in v2 to those of v1
v2.v1(clubb.MG.ZMother)	***v2.v1(clubb.MG)*** + ZM related parameters, except for trigger function, changed from the settings in v2 to those of v1
v2.v1(clubb.MG.ZMother.gust)	***v2.v1(clubb.MG.ZMother)*** + Turn off gustiness parameterization
v2.v1(clubb.MG.ZMother.gust.ZMtrig)	***v2.v1(clubb.MG.ZMother.gust)*** + Turn off the new trigger function
v2.v1(clubb.MG.ZMother.gust.ZMtrig.gw)	***v2.v1(clubb.MG.ZMother.gust.ZMtrig)*** + Gravity wave related parameters changed from the settings in v2 to those of v1
v2.v1(All)	***v2.v1(clubb.MG.ZMother.gust.ZMtrig.gw)*** + so4_sz_thresh (ice nucleation SO2 size threshold for Aitken mode), sea salt and dust emission factors, linoz_psc_t (ozone related)
v1	E3SMv1

Table 3. Description of singly reverted simulations for ZMtrig, MG, CLUBB and ZMother. In the description, the bold italicized text denotes the base experiment and the non-italicized text denotes the added configuration relative to the base experiment. Subgroup experiments for ZMtrig and MG are used to isolate the impact of ULL setting and each MG parameter on cloud feedback changes, respectively.

Short Name	Description	Subgroup experiments
v2.v1(ZMtrig)	***v2*** + ZM trigger function from v1	***v2*** + v1.ZMtrig_ULL (only turn off the ULL setting in the new trigger function)
v2.v1(MG)	***v2*** + all MG parameters from v1	***v2*** + v1.MG_WBF (WBF efficiency) ***v2*** + v1.MG_mincdnc (minimum CDNC) ***v2*** + v1.MG_accre (accretion factor) ***v2*** + v1.MG_auto (autoconversion CDNC exponent) ***v2*** + v1.MG_wsub (subgrid velocity)
v2.v1(clubb)	***v2*** + CLUBB parameters from v1 (same as the 'v2.v1(clubb)' in Table 2)	
v2.v1(ZMother)	***v2*** + ZM other parameters from v1	

To test the impact of individual modifications listed in Table 1 on cloud feedback reduction in v2, we first progressively revert each modification from their v2 values to their v1 values (Table 2) and evaluate their impacts on cloud feedback in each regime as described in Section 2 Methods (Figure 3a). The decreased total cloud feedback from E3SMv1 to E3SMv2 mainly results from the tropical marine low cloud regime, consistent with Figure 2. In the tropical marine low cloud regime, modifications from ZMtrig (not including ZMtrig_ULL), ZMother, MG, and CLUBB all contribute to the reduced total cloud feedback in v2 with a slight compensation from gust. The progressively reverted strategy also reveals the compensating effects between different modifications and regimes. For example, over the midlatitudes, the modifications in MG decrease the cloud feedback and the modifications in ZMtrig increase the cloud feedback. The increase of midlatitude cloud feedback from ZMtrig counteracts its impact on the tropical marine low cloud regime leading to a negligible impact of ZMtrig on the global net cloud feedback change.

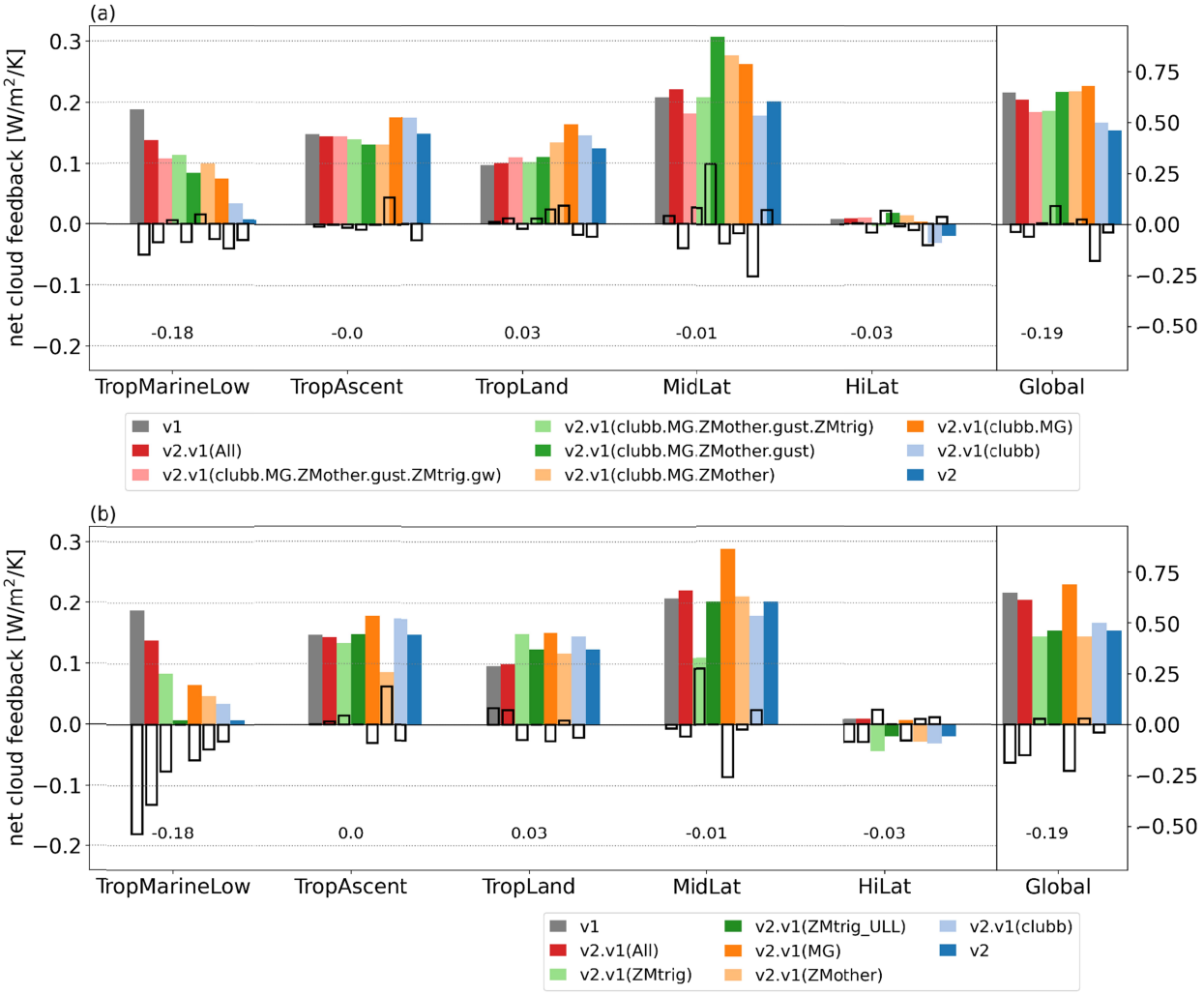

Figure 3. Regime-partitioned total cloud feedback ($W/m^2/K$) (solid bars) for (a) progressively-reverted simulations and (b) singly-reverted simulations. All feedbacks are scaled by the fractional area of each regime so as to represent the contribution to the global mean total cloud feedback. The unfilled bars denote the cloud feedback difference between the two adjacent bars (the right value minus the left value) in (a) and denote the cloud feedback difference between v2 and each simulation (v2 minus the value) in (b). The regime-averaged difference between v2 and v1 is labeled. In panel (b), the subgroup experiment of ZMtrig where ULL is turned off, i.e, ZMtrig_ULL, is also shown as a forest green bar.

The leading contributors identified in these progressively-reverted simulations may depend on the order in which parameterization changes were implemented. Rather than performing all possible permutations of the modification order, we also perform a set of simulations in which we singly revert each modification to their v1 values for clubb, MG, ZMtrig, and ZMothers (Table 3). The results (Figure 3b) show that modifications in MG still

cause the largest reduction of global-mean total cloud feedback. The impact of individual modifications on cloud feedback from singly-reverted simulations is overall larger than that from progressively reverted simulations in the tropical ascent and marine low cloud regimes (Figure 3). The MG modifications still make an important contribution to the cloud feedback reduction in the tropical marine low cloud regime, and modifications in ZMtrig lead to a larger reduction of cloud feedback.

For subsequent detailed analysis of the mechanisms relating individual parameterization changes to changes in cloud feedback, we focus on those parameterization changes that cause large feedback changes in both the progressively and singly reverted simulations shown in Figure 3. Henceforth, we will examine the ZMtrig related modifications (Section 4.1) due to their largest impact on tropical marine low cloud feedback, and the MG-related modifications (Section 4.2) due to their largest impact on global mean cloud feedback and important role in the tropical marine low cloud regime.

Separately, parameter changes in ZMother contribute to the reduced cloud feedback in the tropical ascent cloud regime, which is balanced by the increased cloud feedback due to modifications in MG and CLUBB. Also, the new ZM trigger function leads to a stronger positive cloud feedback over the midlatitudes, which balances out the weakened cloud feedback caused by MG there. Impact of these parameterizations change over these two regimes requires further understanding. However, this paper focuses on understanding those changes that most strongly impact the global mean cloud feedback change from v1 to v2, so these are not analyzed in detail.

4 Physical processes contributing to evolution of cloud feedback from E3SMv1 to E3SMv2

4.1 Deep convection trigger function

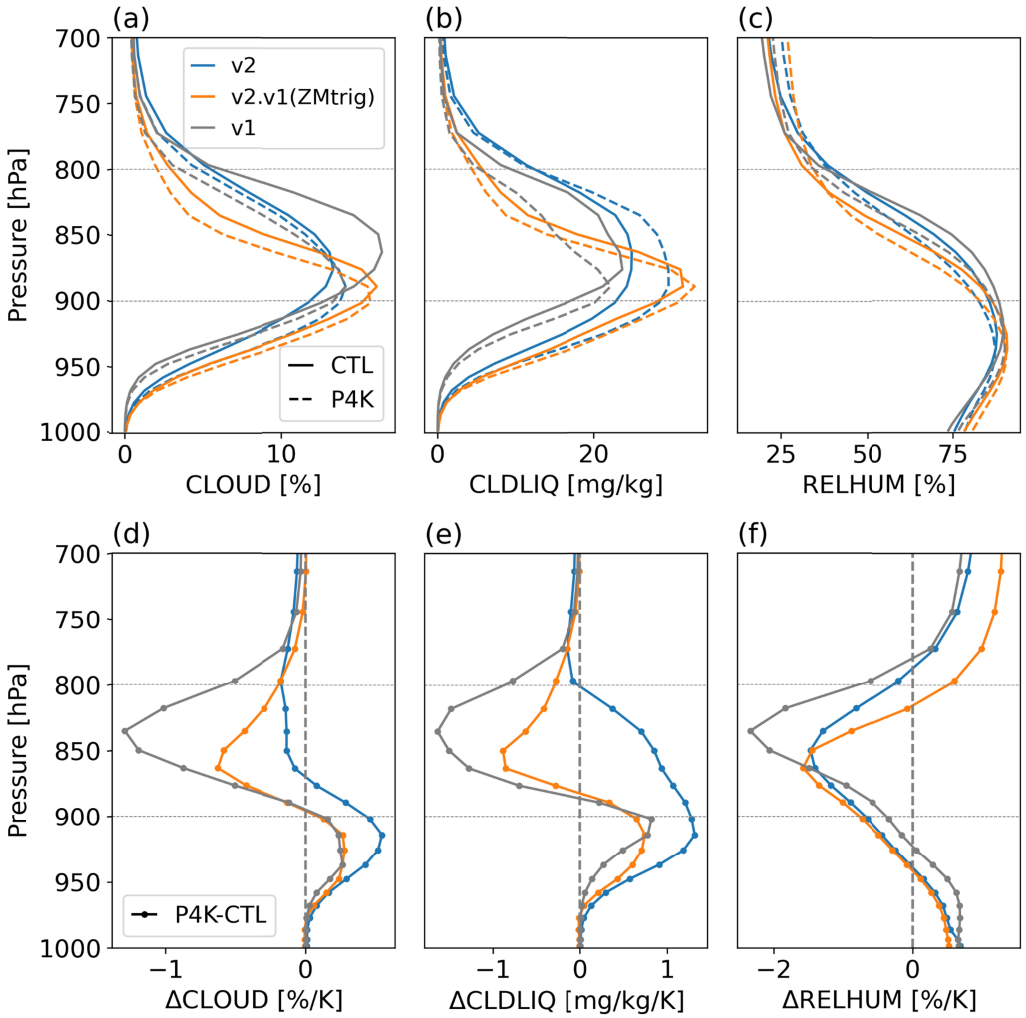

Figure 4. Profiles of cloud fraction (CLOUD), cloud water (CLDLIQ), and relative humidity (RELHUM) from v2, v2.v1(ZMtrig) and v1 averaged over the defined tropical marine low cloud region denoted in Figure S4. The difference between P4K and CTL mediated by global mean surface air temperature anomaly is in (d-f).

Section 3.2 shows that changes to ZM trigger function lead to a weaker positive tropical marine low cloud feedback and a stronger positive midlatitude cloud feedback in v2 compared to v1 (Figure 3 and Figure S4). We further explore the physical processes contributing to this result. First note that the difference in cloud feedback between v2 and v2.v1(ZMtrig) is mostly due to the dCAPE trigger function as the subgroup experiment without the Unrestricted air parcel Launch Level setting (v2.v1(ZMtrig_ULL)) exhibits negligible cloud feedback change (Figure 3b).

In the tropical marine low cloud regime, we examine the mean-state clouds and related variables averaged over a region (10°S-30°S, 80°W-120°W; marked in Figure S4) where the new trigger function leads to the largest cloud feedback reduction. Relative to v1, v2 has a smaller mean state cloud fraction and slightly more cloud water (Figure 4a-b). Under warming, v1 shows a large decrease of cloud fraction and cloud water above 900 hPa. The cloud fraction reduction is weaker in v2 while cloud water is not decreased but increased below 800 hPa in v2 (Figure 4d-e). v2.v1(ZMtrig) shows similar vertical cloud responses as v1 except that cloud reduction is weaker above 900 hPa (Figure 4). The similarity between v2.v1(ZMtrig) and v1 confirms the contribution of ZMtrig to the reduction of tropical marine low cloud feedback from v1 to v2. Compared with v2.v1(ZMtrig), the larger cloud fraction and cloud water in v2 is consistent with the higher relative humidity above 850 hPa (Figure 4a-c). Between 800 and 900 hPa, the cloud fraction and water responses differ the most between v2 and v2.v1(ZMtrig), which is not consistent with the general reduction of relative humidity there (Figure 4f). The opposite response to warming of cloud water and cloud fraction between 800 and 875 hPa in v2 indicates that the new trigger function tends to produce more 'dense' clouds (larger in-cloud water and smaller cloud fraction) with warming. The estimated inversion strength (EIS) response to warming is similar between v2 and v2.v1(ZMtrig) and it is not able to explain the cloud change here (not shown).

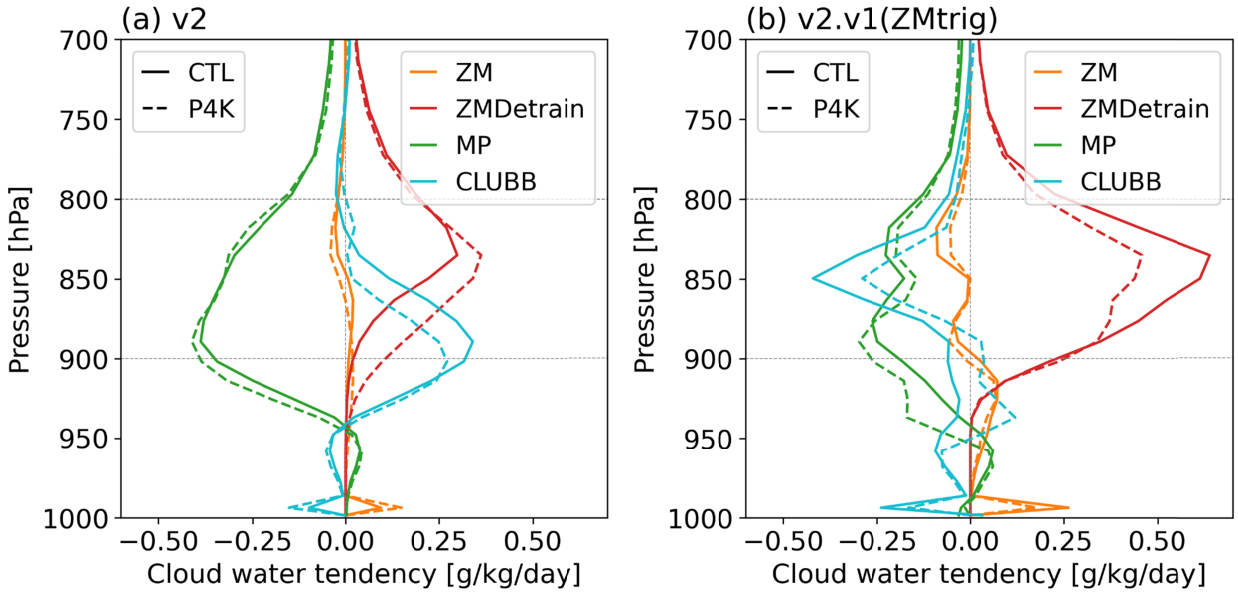

Figure 5. Profiles of tendency terms of cloud water in v2 and v2.v1(ZMtrig) over the defined marine low cloud region denoted in Figure S4. The CTL is in solid line and P4K is in dashed line. ZM: ZM deep convection except the detrainment; ZMDetrain: detrainment from ZM deep convection; MP: cloud microphysics.

To better understand the impact of the ZM trigger function on cloud responses between v2 and v2.v1(ZMtrig), especially between 800 and 900 hPa, the cloud water tendencies from different physical schemes are examined in Figure 5. For v2, the detrainment from ZM deep convection (ZMDetrain) and CLUBB are major cloud water sources, balanced by the sink from cloud microphysics (MP). For v2.v1(ZMtrig), the detrainment from ZM deep convection is almost the only cloud water source, indicating the ZM deep convection is very active even over this marine low cloud region. Both MP and CLUBB are cloud water sinks in v2.v1(ZMtrig). Therefore, the cloud water change under warming depends on the change of the relative contributions of these sources and sinks. Under warming, the cloud water detrainment from ZM deep convection gets weaker between 800 and 900 hPa in v2.v1(ZMtrig) but gets larger in v2, consistent with the increased cloud water there (Figure 4e). We conclude that the different responses of cloud water detrainment from ZM deep convection lead to the different cloud water change with warming in v2 relative to v2.v1(ZMtrig).

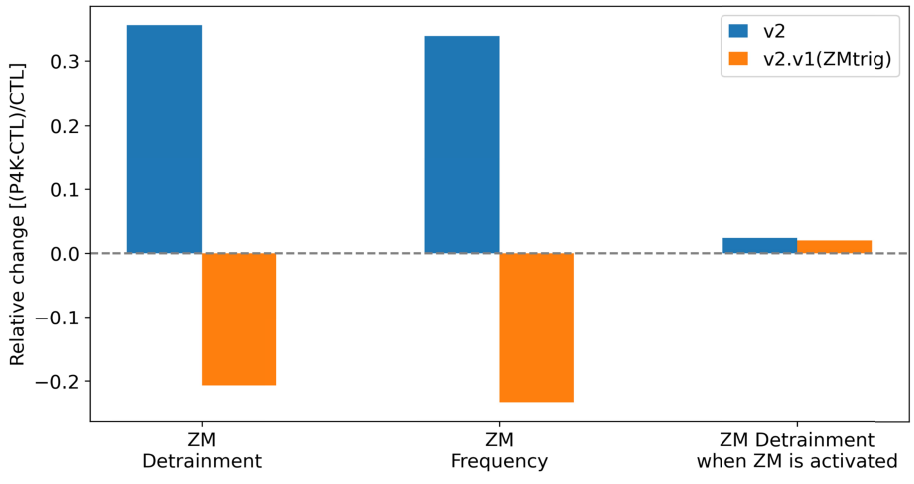

Figure 6. Relative change of the vertically-integrated (surface to 700 hPa) detrainment of cloud water from ZM deep convection (ZM Detrainment), occurrence frequency of ZM convection

(ZM Frequency), and the vertically-integrated (surface to 700 hPa) ZM detrainment when ZM is activated from v2 and v2.v1(ZMtrig) over the defined marine low cloud region.

The differing response of ZM detrainment may come either from changes in the frequency that the ZM scheme is active or the amount of cloud water that is detrained when the ZM scheme is active. We examine the relative contributions from changes in the ZM frequency and changes in ZM detrainment when ZM is activated in v2 and v2.v1(ZMtrig) in Figure 6. Over the defined tropical marine low cloud region, the mean-state ZM frequency is about 16% in v2 and 35% in v2.v1(ZMtrig) respectively (not shown), which is consistent with the finding that the more restrictive conditions of the dCAPE-based trigger function tend to reduce the convective-to-total precipitation ratios in the subtropics (Xie et al., 2019). Whereas the average ZM detrainment for the ZM-activated period increases with warming by roughly the same amount in v2 and v2.v1(ZMtrig), the ZM frequency increases by roughly 30% in v2 but decreases by roughly 20% in v2.v1(ZMtrig). Therefore, we conclude that, under warming, the increased cloud water detrainment due to increased ZM frequency is the main contributor to the cloud water increase, leading to a weaker cloud feedback in v2 compared to v2.v1(ZMtrig).

The activation of ZM convection in v2 relies on the presence of positive values for both CAPE and dCAPE (Xie et al., 2019). In our analysis of one-year simulations with hourly output for v2 over the defined marine low cloud region, we find that dCAPE values greater than zero are always accompanied by CAPE values greater than zero in both the CTL and P4K experiments (Table S2). This implies that changes in dCAPE have a greater influence on the change of ZM frequency with warming than do changes in CAPE. Indeed, the occurrence of dCAPE values greater than zero increases with warming, indicating that the large-scale environment is more favorable for convection in a warmer climate. Additional investigation is required to understand why the occurrence of dCAPE values greater than zero increases with warming. In v2.v1(ZMtrig), the reduced frequency of convection is primarily due to weakened CAPE values with warming. Specifically, values less than 70 J/kg become more frequent (Table S3). This is likely caused by the increased lower tropospheric stability (Chen et al., 2020; Qu et al., 2015), which inhibits the generation of CAPE.

399 4.2 Microphysics

400 Section 3.2 indicates that modifications in MG significantly affect the global mean cloud
401 feedback (Figure 3), not only in tropical marine low cloud regime, but also in midlatitudes.
402 Relative to v1, the MG modifications in v2 include an increased Wegener-Bergeron-Findeisen
403 process (WBF) factor, an added threshold of a minimum cloud droplet number concentration
404 (CDNC), a reduced minimum subgrid-scale vertical velocity for aerosol activation, an increased
405 accretion rate enhancement factor, and a greater dependence of the auto-conversion rate on the
406 liquid CDNC. The minimum CDNC threshold (10 cm^{-3}) prevents the occurrence of clouds with
407 nonzero cloud fraction but very few cloud droplets. This threshold is also used in ECHAM6.3
408 (Salzmann et al., 2022) and showed impacts on aerosol effective radiative forcing and EffCS
409 (Neubauer et al., 2019). The more negative autoconversion CDNC exponent enhances the
410 sensitivity of autoconversion rate to a CDNC change, and the increased accretion enhancement
411 factor increases the accretion rate of cloud droplets by rain. To isolate their relative contributions
412 to the global cloud feedback, we conducted a set of subgroup experiments with one modification
413 at a time (Table 3).

414

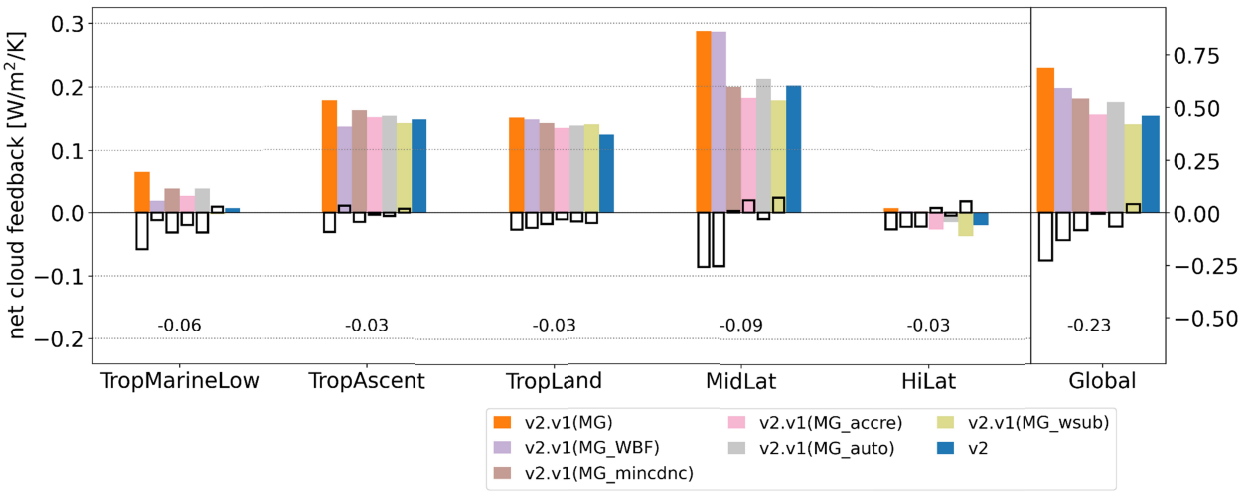

415

416 **Figure 7.** Contributions of WBF factor (MG_WBF), minimum CDNC threshold (MG_mincdnc),
417 accretion factor (MG_accre), autoconversion CDNC exponent (MG_auto) and all MG
418 modifications (MG) on total cloud feedback changes in each cloud regime. The unfilled bars
419 denote the cloud feedback difference between v2 and each simulation (v2 minus the value). The
420 differences between v2 and v2.v1(MG) are labeled as the text in the lower part.

421

As shown by v2.v1(MG), the total effect of all MG modifications reduces the global net cloud feedback by 0.23 $W/m^2/K$ with the main contributions coming from the tropical marine low cloud regime and midlatitudes. In the tropical marine low cloud regime, all individual modifications except MG_wsub contribute to the reduced net cloud feedback (Figure 7). Note that the slightly weakened positive cloud feedback due to the increased WBF factor in this regime mainly results from the high cloud changes, because the definition of the tropical marine low cloud regime here uses the climatological vertical velocity at 700 hPa and some high clouds infrequently occur. Over midlatitudes, the reduced net cloud feedback mainly results from the increased WBF factor, which increases the conversion efficiency from cloud liquid to ice.

In the tropical marine low cloud regime, interestingly, all modifications except the tuned accretion factor and autoconversion CDNC exponent have negligible effects on the mean-state cloud profiles. Their warming responses, however, are quite different. Each modification except MG_wsub contributes to the reduced net cloud feedback by suppressing the cloud fraction reduction and enhancing the cloud liquid water increase mainly between 800 and 900 hPa (Figure 8 and Figure S5). The minimum CDNC threshold and more negative autoconversion CDNC exponent have slightly larger impacts than others (Figure 7 and Figure 8d-e). We focus now on explaining why these two changes reduce the cloud feedback in this regime.

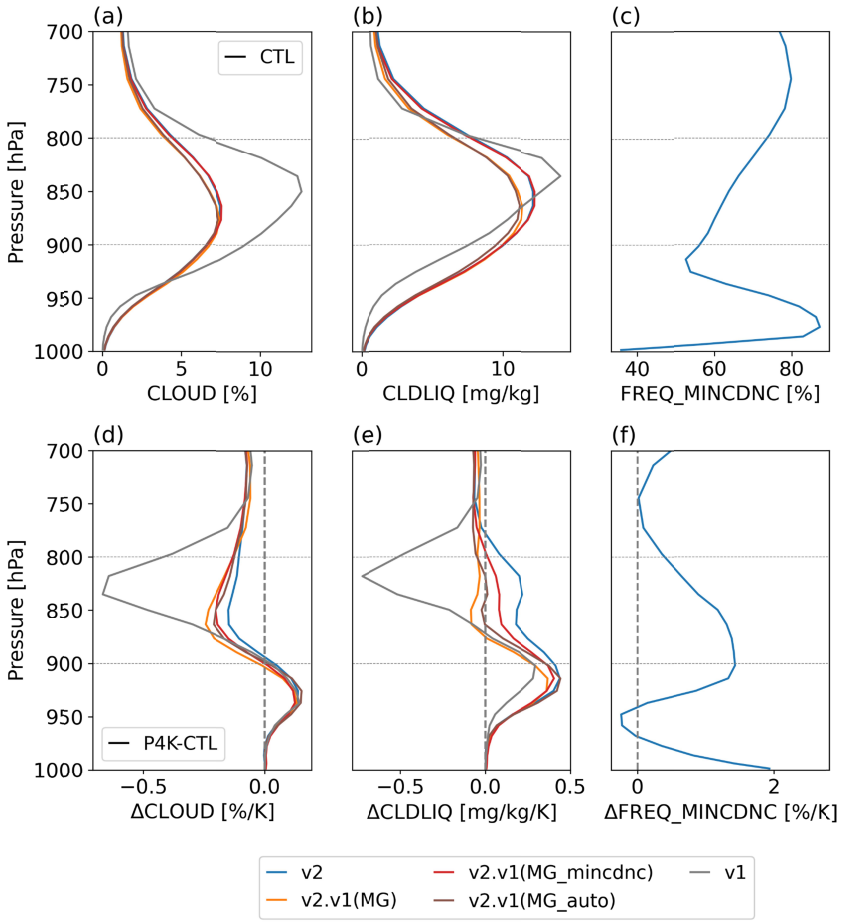

Figure 8. Profiles of (a) cloud fraction (CLOUD; %), (b) cloud water (CLDLIQ; mg/kg) and (c) occurrence frequency of in-cloud CDNC lower than 10 cm^{-3} (FREQ_MINCDNC; %) from v1, v2, v2.v1(MG), v2.v1(MG_mincdnc) and v2.v1(MG_auto) averaged over the tropical marine low cloud regime. The difference between P4K and CTL mediated by the global mean surface air temperature anomaly is in (d-f). FREQ_MINCDNC and its warming response are only available from v2.

With regard to the autoconversion CDNC exponent, the autoconversion rate ($A_u = k * (cloud\ water\ content)^a * (CDNC)^b$) is reduced when the autoconversion CDNC exponent b is changed from -1.2 to -1.4, if everything else is unchanged. We will henceforth use the term "reduced autoconversion" to refer to the effects of the more negative autoconversion CDNC exponent. To further understand its impact on weakened positive cloud feedback, we examine the cloud water tendencies and their responses with warming in the tropical marine low cloud regime. The cloud water from CLUBB and detrainment from deep convection are the main cloud water sources, and the cloud microphysics (MG) is the only cloud water sink. The cloud water removal by MG is dominated by the cloud water to precipitation process, which includes the

autoconversion from liquid water to rain and cloud water accretion by rain. The tendency from accretion by rain and autoconversion dominates the total tendency of cloud water to precipitation (Figure 9a). In v2, the reduced autoconversion causes a weakened cloud water removal (precipitation suppression) by MG cloud microphysics, mainly balanced by the weakened cloud water production from CLUBB (Figure 9b-c). The suppressed cloud water to precipitation is mainly induced by the weakened accretion by rain and autoconversion from cloud water to rain. The weaker precipitation production due to the reduced autoconversion is consistent with the larger mean-state cloud water in v2 relative to v2.v1(MG_auto) (Figure 8b).

Under warming, the cloud water removal by MG is stronger, which is balanced by the stronger cloud water source from ZM detrainment and weakened cloud water source from CLUBB (Figure 9c). The stronger cloud water source from ZM detrainment is associated with the increased frequency of ZM deep convection with the new dCAPE-based trigger function as discussed in Section 4.1. The reduced autoconversion in v2 weakens the autoconversion and accretion, leading to weaker cloud water removal by precipitation under warming. Indeed for the difference between v2 and v2.v1(MG_auto) in the change in microphysics tendencies with warming (Figure 9d), the autoconversion term is of positive sign meaning that cloud water relatively increases with warming due to the reduced autoconversion. Therefore, the reduced autoconversion (more negative autoconversion CDNC exponent) in v2 suppresses the mean-state precipitation, and this suppression effect gets stronger in a warmer climate, helping sustain the cloud, and leading to a less positive cloud feedback in the tropical marine low cloud regime.

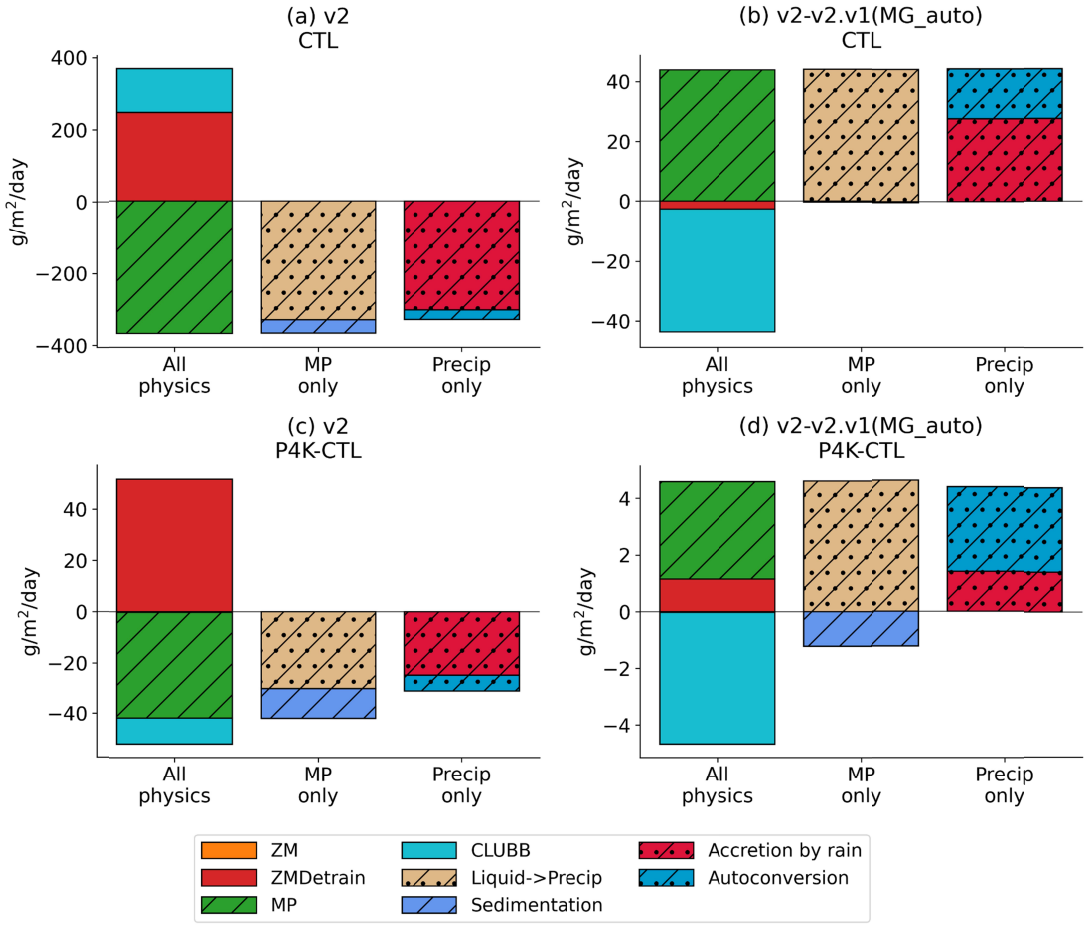

Figure 9. Vertically-integrated cloud water tendencies (surface to 700 hPa) in CTL (a-b) and their warming responses (c-d) in v2 (a&c), and the difference between v2 and v2.v1(MG_auto) (b&d) averaged over the tropical marine low cloud regime. ZM: tendency except the ZM detrainment; ZMDetrain: detrainment from ZM deep convection; MP: cloud microphysics. The MP tendency (second bar in each panel) can be further decomposed into tendencies from sedimentation, liquid to precipitation, liquid to ice (not shown), and liquid to vapor (not shown). The liquid to precipitation tendency (third bar in each panel) is further decomposed into accretion of cloud water by rain, autoconversion of cloud water to rain, accretion of cloud water by snow (not shown) and conversion of cloud water to snow from WBF (not shown). Some terms are not shown because those processes do not largely contribute to the cloud water tendency over the tropical marine low cloud regime.

The minimum CDNC threshold has negligible impact on mean-state cloud fraction and cloud water (Figure 8a-b), but is able to suppress their reduction under warming. We hypothesize that compared to the simulation without the minimum CDNC threshold, the simulation with the introduced minimum CDNC threshold can suppress the cloud reduction under warming if the occurrence frequency of CDNC lower than 10 cm^{-3} tends to occur more frequently under

warming. Implicit in this hypothesis is the notion that increasing CDNC to 10 cm^{-3} right before microphysics is calculated reduces the generation of precipitation via autoconversion and hence supports greater cloud liquid. To examine this, we calculate the frequency of CDNC lower than 10 cm^{-3} (FREQ_MINCDNC), which is assigned a value of 1 when the minimum CDNC threshold is applied and 0 when it is not applied for each time step. The frequency is determined only when clouds are present to exclude the impact of cloud fraction response to warming on the frequency estimate. In the tropical marine low cloud regime, FREQ_MINCDNC is mostly above 60%. This large value may be because CDNC lower than 10 cm^{-3} happens preferentially when cloud fraction is smaller than 10% (not shown), which is very common in marine low cloud regions. Under warming, FREQ_MINCDNC increases by 1-2%/K below 800 hPa. This suggests that more clouds are forced to increase their CDNC from <10 cm^{-3} to 10 cm^{-3}, likely resulting in weaker cloud reduction in a warmer climate. We also examine the precipitation efficiency index defined as the ratio of surface precipitation to the liquid water path (Li et al., 2022) and find the mean-state precipitation efficiency index in v2 is slightly smaller than that in v2.v1(MG_mincdnc) in the tropical marine low cloud regime. Under warming, the precipitation efficiency index is indeed reduced in v2 but almost unchanged in v2.v1(MG_mincdnc) (not shown). Therefore, under warming, the increased occurrence frequency of CDNC lower than 10 cm^{-3} likely leads to a reduced precipitation efficiency (precipitation suppression), weaker cloud reduction, and hence a weaker positive cloud feedback.

Turning to the large impact of the increased WBF factor on the midlatitude cloud feedback (Figure 7), this has partly been explained via a cloud phase feedback in which warming favors the occurrence of more reflective liquid clouds rather than less-reflective ice clouds (Ceppi et al., 2016; McCoy et al., 2015; Mitchell et al., 1989; Mülmenstädt et al., 2021). To investigate whether this mechanism could explain the varying midlatitude cloud feedback strength among these MG sensitivity experiments, the relation between T5050 (the temperature at which the Liquid Condensate Fraction (LCF) equals 0.5) (McCoy et al., 2015) and net cloud feedback over the midlatitudes (30°N-60°N and 30°S-60°S) is examined in Figure 10. Notably, the T5050 increases from 248 K in v2.v1(MG) to 258 K in v2, primarily due to the increased WBF factor in v2. The increased T5050 indicates the mean-state liquid fraction is reduced in v2, which can be confirmed by v2's reduced mean-state cloud water in the mixed-phase temperature region (0 ~ -40°C) relative to v2.v1(MG_Berg) (Figure 11c). Midlatitude cloud water reduces

526 under warming but this reduction is weaker in v2 compared to v2.v1(MG_Berg) (Figure 11e-f),
527 and leads to a weaker positive cloud optical depth feedback (Figure 10). This is consistent with
528 the previous findings that smaller mean-state liquid fraction tends to cause more negative
529 midlatitude cloud feedback (Bodas-Salcedo et al., 2019; Frey et al., 2017; Gettelman et al.,
530 2019).
531

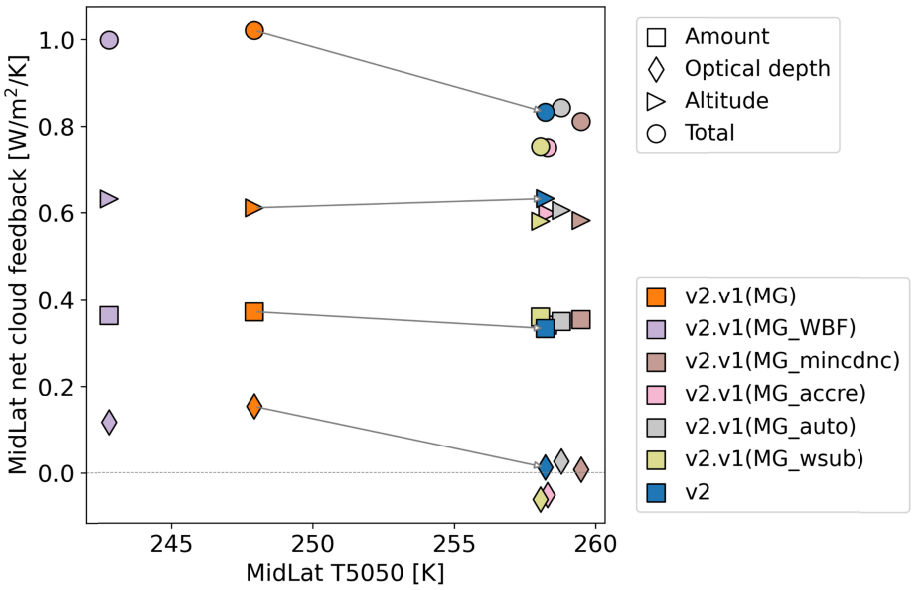

532

533 **Figure 10.** Scatterplot of the total net cloud feedback (W/m^2/K) and its subcomponents due to
534 changes in cloud amount, optical depth, and altitude versus T5050 (K) for v2, v2.v1(MG), and
535 five subgroup sensitivity experiments over the midlatitudes.
536
537

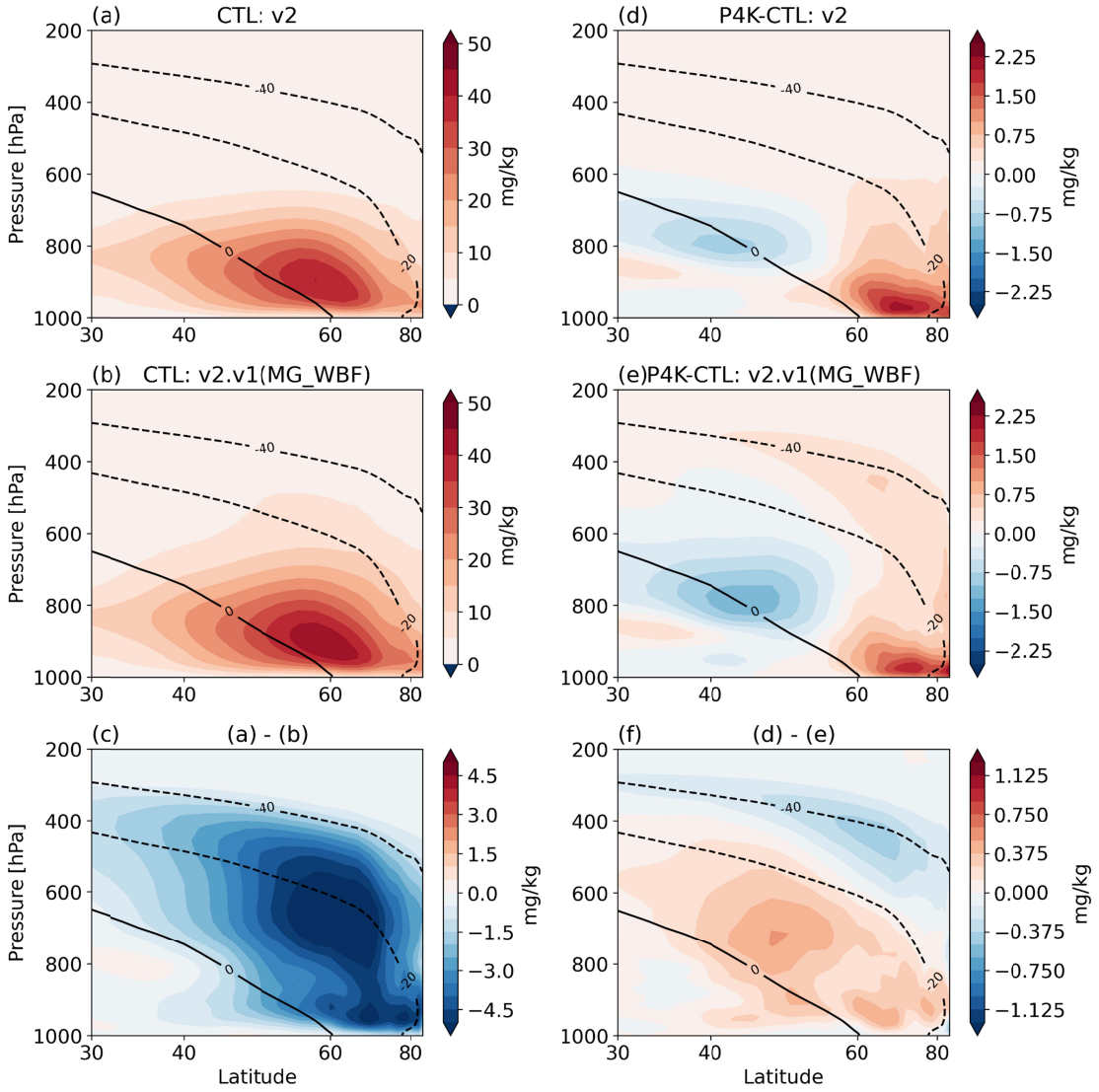

Figure 11. Pressure-Latitude cross section of grid-mean cloud liquid water (mg/kg) from v2 (a&d), v2.v1(MG_WBF) (b&e), and the difference between v2.v1(MG_WBF) and v2 (c&f) in CTL (a-c) and the difference between P4K and CTL (d-f) averaged over the northern and southern hemispheres for middle to high latitudes (30-90 °N/S). The black curves denote the temperature at 0, -20, and -40 ℃ in the control experiment.

5. Conclusions and discussion

This paper investigates the reduction in effective climate sensitivity from 5.3 K in E3SMv1 to 4.0 K in E3SMv2. We find the reduced climate sensitivity is related to both the reduced effective radiative forcing from 4xCO2 and climate feedback, with around 80% of the change attributable to the reduced radiative feedback. The reduced radiative feedback, in turn, is

550 primarily due to a weaker positive cloud feedback, especially over the tropical marine low cloud
551 regime. We further examine the impact of modifications in each physical parameterization on
552 cloud feedbacks by conducting a series of atmosphere-only perturbed SST experiments, and find
553 the modified parameters in MG microphysics and the incorporation of a new trigger function in
554 the ZM deep convection scheme are key to reducing the cloud feedback in E3SMv2 relative to
555 that in E3SMv1.

556 The dilute CAPE trigger function in the ZM deep convection scheme in E3SMv1 is
557 replaced by the dilute dCAPE based trigger function in E3SMv2, which effectively reduces the
558 mean-state occurrence frequency of ZM deep convection in the tropical marine low cloud
559 regime. Under warming, simulations with the new trigger function tend to have more cloud water
560 detrainment from ZM deep convection in the tropical marine low cloud regime, which helps to
561 sustain the clouds and thus leads to less positive marine cloud feedback. The reason for this is a
562 warming-induced increase in the occurrence frequency of ZM deep convection rather than an
563 increase in the mass of condensate detrained when ZM is activated. Further investigation is
564 required to determine the meteorological conditions driving the increased occurrence frequency
565 of dCAPE larger than zero with warming in the new trigger function. For v2, the introduced
566 minimum cloud droplet number concentration (CDNC) threshold and more negative
567 autoconversion CDNC exponent in MG both lead to a less positive marine low cloud feedback.
568 These two modifications help sustain clouds by suppressing precipitation from MG in the mean
569 state, and enhancing the precipitation suppression under warming in the tropical marine low
570 cloud regime. Lastly, the increased scaling factor of the Wegener-Bergeron-Findeisen (WBF)
571 process from E3SMv1 to E3SMv2 converts the liquid to ice more efficiently, leading to less
572 supercooled liquid cloud water in the mean state and a weaker cloud water reduction under
573 warming. This is the dominant reason that the positive midlatitude cloud feedback weakens in
574 v2. This is consistent with the previous finding that models with less present-day supercooled
575 water tend to produce a more negative cloud phase feedback.

576 How well do individual cloud feedbacks simulated by E3SMv2 match those determined
577 through expert judgment informed by multiple lines of evidence, and is there any improvement
578 with respect to E3SMv1? Following Zelinka et al (2022), we further compare the cloud feedback
579 components from E3SMv1 and E3SMv2 with the expert assessment of cloud feedback
580 components of Sherwood et al (2020). The reduced total cloud feedback in v2 mainly results

from the tropical marine low cloud regime, and the tropical marine low cloud feedback in E3SMv2 appears to be too weak compared to the expert assessment (Figure S6). However, recent studies using large eddy simulations (LES) and satellite and in-situ observations suggest smaller trade cumulus cloud feedbacks than reported in the expert assessment (Cesana & Del Genio, 2021; Myers et al., 2021; Radtke et al., 2021; Vogel et al., 2022), suggesting that the tropical marine low cloud feedback in v2 may be more reasonable than that of v1. Indeed, following the regime definitions of Myers et al (2021), we find that v2 produces a trade cumulus cloud feedback around 0.05 $W/m^2/K$, much closer to the observationally-constrained estimates of Myers et al. (2021) than those produced in v1 (0.17 $W/m^2/K$). The stratocumulus cloud feedback is also reduced in v2 compared with v1, yet it deviates further from the estimate derived from observational constraints. This suggests that further process-oriented evaluation of cloud feedback and its components during the model development is needed.

With regard to the physical mechanisms explaining the trade cumulus cloud feedback, recent studies have revealed that, unlike many climate models, the trade cumulus cloud amount at the cloud base remains unchanged in a warmer world (Blossey et al., 2016; Vogel et al., 2016). The climate models with too strong trade cumulus cloud feedback (Cesana & Del Genio, 2021; Sherwood et al., 2014) tend to show unrealistically decreased cloudiness near the cloud base (Vial et al., 2017) through an increase in convective mixing with warming. The enhanced convective mixing lowers the relative humidity and cloudiness near the cloud base ('mixing-desiccation' mechanism in Vogel et al., 2022). However, mesoscale circulations (absent in climate models) might counteract this drying, leading to a stabilization of clouds near the cloud base ('mesoscale motion control' in Vogel et al., 2022), and thus a weak trade cumulus cloud feedback. E3SM (either v1 or v2), in contrast, does not seem to have the 'mixing-desiccation' issue present in some climate models. Both cloud fraction and cloud water at the cloud base slightly increase with warming (Figure 4 and Figure 8), and reductions in cloud fraction and relative humidity tend to happen in the upper part of the cloud layer, and not at the cloud base. The shoaling cloud layer occurs in all E3SM sensitivity experiments, not revealed in LES and observations, is likely related to the shallower boundary layer and weakened turbulent mixing under warming due to the CLUBB scheme. Zhang et al. (2018) also found the turbulent mixing tends to decrease under warming in CAM5-CLUBB, and the weakened turbulent mixing is mainly caused by the reduced buoyancy flux near the cloud base. Furthermore, the frequency of

612 ZM deep convection increases with warming, but it leads to more, not less clouds, through
613 increased convective detrainment in v2. Therefore, while the value of v2's weaker trade cumulus
614 feedback is more consistent with observation evidence and LES, we cannot say that this change
615 results from an improved simulation of how physical processes respond to climate warming.
616 Nonetheless, some of the process changes between v1 and v2 (such as the ZM trigger function or
617 the WBF process factor) improve the agreement with present-day observations of process-related
618 variables (such as the diurnal cycle of precipitation or the amount of supercooled liquid,
619 respectively), and on this basis one might have greater confidence that the reduced cloud
620 feedback exhibited under climate warming in v2 is more realistic. Overall, continued research
621 and analysis are needed to better understand the complex interactions among model physics and
622 to refine parameterizations in climate models for more accurate representation of these processes
623 in future climate projections.

624

625 **Acknowledgments**

626 We thank Karl Taylor for the useful comments and discussion on this work. This research
627 is supported by the U.S. Department of Energy, Office of Science, Office of Biological and
628 Environmental Research. The work of Y.Q., M.D.Z., S.A.K. and P.M. is supported by its
629 Regional and Global Climate Modeling Program. J.-C.G., S.X. and X.Z. are supported by its
630 Energy Exascale Earth System Model (E3SM) project. Work at Lawrence Livermore National
631 Laboratory was performed under the auspices of the U.S. Department of Energy by Lawrence
632 Livermore National Laboratory under contract DE-AC52-07NA27344. The Pacific Northwest
633 National Laboratory is operated for the U.S. Department of Energy by the Battelle Memorial
634 Institute under contract DE-AC05-76RL01830. Simulations were performed using BER ESM
635 program's Compy computing cluster located at Pacific Northwest National Laboratory.

636

637 **Data Availability Statement**

638 The model codes can be accessed from https://github.com/E3SM-Project/E3SM.
639 Maintenance branches maint-1.0 (https://github.com/E3SM-Project/E3SM/tree/maint-1.0) and
640 maint-2.0 (https://github.com/E3SM-Project/E3SM/tree/maint-2.0) are used for reproducing
641 simulations of version 1 and version 2, respectively. All simulation data including run scripts can

be accessed from https://portal.nersc.gov/archive/home/projects/mp193/www/qinyi/E3SM_CFBK_v1v2. CMIP model data used in Figure 1 are from DOE Earth System Grid Federation (ESGF) at https://esgf-node.llnl.gov/.

References

Beres, J. H., Alexander, M. J., & Holton, J. R. (2004). A Method of Specifying the Gravity Wave Spectrum above Convection Based on Latent Heating Properties and Background Wind. *Journal of the Atmospheric Sciences*, *61*(3), 324–337. https://doi.org/10.1175/1520-0469(2004)061<0324:AMOSTG>2.0.CO;2

Blossey, P. N., Bretherton, C. S., Cheng, A., Endo, S., Heus, T., Lock, A. P., & van der Dussen, J. J. (2016). CGILS Phase 2 LES intercomparison of response of subtropical marine low cloud regimes to CO2 quadrupling and a CMIP3 composite forcing change. *Journal of Advances in Modeling Earth Systems*, *8*(4), 1714–1726. https://doi.org/10.1002/2016MS000765

Bodas-Salcedo, A., Mulcahy, J. P., Andrews, T., Williams, K. D., Ringer, M. A., Field, P. R., & Elsaesser, G. S. (2019). Strong Dependence of Atmospheric Feedbacks on Mixed-Phase Microphysics and Aerosol-Cloud Interactions in HadGEM3. *Journal of Advances in Modeling Earth Systems*, *11*(6), 1735–1758. https://doi.org/10.1029/2019MS001688

Ceppi, P., Hartmann, D. L., & Webb, M. J. (2016). Mechanisms of the Negative Shortwave Cloud Feedback in Middle to High Latitudes. *Journal of Climate*, *29*(1), 139–157. https://doi.org/10.1175/JCLI-D-15-0327.1

Cesana, G. V., & Del Genio, A. D. (2021). Observational constraint on cloud feedbacks suggests moderate climate sensitivity. *Nature Climate Change*, *11*(3), 213–218. https://doi.org/10.1038/s41558-020-00970-y

Chen, J., Dai, A., Zhang, Y., & Rasmussen, K. L. (2020). Changes in Convective Available Potential Energy and Convective Inhibition under Global Warming. *Journal of Climate*, *33*(6), 2025–2050. https://doi.org/10.1175/JCLI-D-19-0461.1

Forster, P., Storelvmo, T., Armour, K., Collins, W., Dufresne, J. L., Frame, D., Lunt, D. J., Mauritsen, T., Palmer, M. D., Watanabe, M., Wild, M., & Zhang, H. (2021). The Earth's Energy Budget, Climate Feedbacks, and Climate Sensitivity. In V. Masson-Delmotte, P. Zhai, A. Pirani, S. L. Connors, C. Péan, S. Berger, N. Caud, Y. Chen, L. Goldfarb, M. I. Gomis, M. Huang, K. Leitzell, E. Lonnoy, J. B. R. Matthews, T. K. Maycock,

T. Waterfield, O. Yelekçi, R. Yu, & B. Zhou (Eds.), *Climate Change 2021: The Physical Science Basis. Contribution of Working Group I to the Sixth Assessment Report of the Intergovernmental Panel on Climate Change*. Cambridge University Press. https://www.ipcc.ch/report/ar6/wg1/downloads/report/IPCC_AR6_WGI_Chapter_07.pdf

Frey, W. R., Maroon, E. A., Pendergrass, A. G., & Kay, J. E. (2017). Do Southern Ocean Cloud Feedbacks Matter for 21st Century Warming? *Geophysical Research Letters*, *44*(24), 12,447-12,456. https://doi.org/10.1002/2017GL076339

Gettelman, A., Hannay, C., Bacmeister, J. T., Neale, R. B., Pendergrass, A. G., Danabasoglu, G., Lamarque, J. -F., Fasullo, J. T., Bailey, D. A., Lawrence, D. M., & Mills, M. J. (2019). High Climate Sensitivity in the Community Earth System Model Version 2 (CESM2). *Geophysical Research Letters*, *46*(14), 8329–8337. https://doi.org/10.1029/2019GL083978

Gettelman, A., Kay, J. E., & Shell, K. M. (2012). The Evolution of Climate Sensitivity and Climate Feedbacks in the Community Atmosphere Model. *Journal of Climate*, *25*(5), 1453–1469. https://doi.org/10.1175/JCLI-D-11-00197.1

Gettelman, A., & Morrison, H. (2015). Advanced Two-Moment Bulk Microphysics for Global Models. Part I: Off-Line Tests and Comparison with Other Schemes. *Journal of Climate*, *28*(3), 1268–1287. https://doi.org/10.1175/JCLI-D-14-00102.1

Golaz, J., Caldwell, P. M., Van Roekel, L. P., Petersen, M. R., Tang, Q., Wolfe, J. D., Abeshu, G., Anantharaj, V., Asay-Davis, X. S., Bader, D. C., Baldwin, S. A., Bisht, G., Bogenschutz, P. A., Branstetter, M., Brunke, M. A., Brus, S. R., Burrows, S. M., Cameron-Smith, P. J., Donahue, A. S., … Zhu, Q. (2019). The DOE E3SM Coupled Model Version 1: Overview and Evaluation at Standard Resolution. *Journal of Advances in Modeling Earth Systems*, *11*(7), 2089–2129. https://doi.org/10.1029/2018MS001603

Golaz, J., Van Roekel, L. P., Zheng, X., Roberts, A. F., Wolfe, J. D., Lin, W., Bradley, A. M., Tang, Q., Maltrud, M. E., Forsyth, R. M., Zhang, C., Zhou, T., Zhang, K., Zender, C. S., Wu, M., Wang, H., Turner, A. K., Singh, B., Richter, J. H., … Bader, D. C. (2022). The DOE E3SM Model Version 2: Overview of the Physical Model and Initial Model Evaluation. *Journal of Advances in Modeling Earth Systems*, *14*(12). https://doi.org/10.1029/2022MS003156

697 Golaz, J.-C., Larson, V. E., & Cotton, W. R. (2002). A PDF-Based Model for Boundary Layer Clouds. Part I:
698 Method and Model Description. *Journal of the Atmospheric Sciences*, *59*(24), 3540–3551.
699 https://doi.org/10.1175/1520-0469(2002)059<3540:APBMFB>2.0.CO;2
700 Gregory, J. M., Ingram, W. J., Palmer, M. A., Jones, G. S., Stott, P. A., Thorpe, R. B., Lowe, J. A., Johns, T. C., &
701 Williams, K. D. (2004). A new method for diagnosing radiative forcing and climate sensitivity.
702 *Geophysical Research Letters*, *31*(3), L03205. https://doi.org/10.1029/2003GL018747
703 Hansen, J., Sato, M., Ruedy, R., Nazarenko, L., Lacis, A., Schmidt, G. A., Russell, G., Aleinov, I., Bauer, M.,
704 Bauer, S., Bell, N., Cairns, B., Canuto, V., Chandler, M., Cheng, Y., Del Genio, A., Faluvegi, G., Fleming,
705 E., Friend, A., … Zhang, S. (2005). Efficacy of climate forcings. *Journal of Geophysical Research*,
706 *110*(D18), D18104. https://doi.org/10.1029/2005JD005776
707 Harrop, B. E., Ma, P., Rasch, P. J., Neale, R. B., & Hannay, C. (2018). The Role of Convective Gustiness in
708 Reducing Seasonal Precipitation Biases in the Tropical West Pacific. *Journal of Advances in Modeling*
709 *Earth Systems*, *10*(4), 961–970. https://doi.org/10.1002/2017MS001157
710 Held, I. M., & Shell, K. M. (2012). Using Relative Humidity as a State Variable in Climate Feedback Analysis.
711 *Journal of Climate*, *25*(8), 2578–2582. https://doi.org/10.1175/JCLI-D-11-00721.1
712 Larson, V. E. (2017). *CLUBB-SILHS: A parameterization of subgrid variability in the atmosphere*.
713 https://doi.org/10.48550/ARXIV.1711.03675
714 Li, R. L., Studholme, J. H. P., Fedorov, A. V., & Storelvmo, T. (2022). Precipitation efficiency constraint on climate
715 change. *Nature Climate Change*, *12*(7), Article 7. https://doi.org/10.1038/s41558-022-01400-x
716 Ma, P.-L., Harrop, B. E., Larson, V. E., Neale, R. B., Gettelman, A., Morrison, H., Wang, H., Zhang, K., Klein, S.
717 A., Zelinka, M. D., Zhang, Y., Qian, Y., Yoon, J.-H., Jones, C. R., Huang, M., Tai, S.-L., Singh, B.,
718 Bogenschutz, P. A., Zheng, X., … Leung, L. R. (2022). Better calibration of cloud parameterizations and
719 subgrid effects increases the fidelity of the E3SM Atmosphere Model version 1. *Geoscientific Model*
720 *Development*, *15*(7), 2881–2916. https://doi.org/10.5194/gmd-15-2881-2022
721 McCoy, D. T., Hartmann, D. L., Zelinka, M. D., Ceppi, P., & Grosvenor, D. P. (2015). Mixed-phase cloud physics
722 and Southern Ocean cloud feedback in climate models. *Journal of Geophysical Research: Atmospheres*,
723 *120*(18), 9539–9554. https://doi.org/10.1002/2015JD023603

724 Mitchell, J. F. B., Senior, C. A., & Ingram, W. J. (1989). C02 and climate: A missing feedback? *Nature*, *341*(6238),
725 132–134. https://doi.org/10.1038/341132a0
726 Morrison, H., & Gettelman, A. (2008). A New Two-Moment Bulk Stratiform Cloud Microphysics Scheme in the
727 Community Atmosphere Model, Version 3 (CAM3). Part I: Description and Numerical Tests. *Journal of*
728 *Climate*, *21*(15), 3642–3659. https://doi.org/10.1175/2008JCLI2105.1
729 Mülmenstädt, J., Salzmann, M., Kay, J. E., Zelinka, M. D., Ma, P.-L., Nam, C., Kretzschmar, J., Hörnig, S., &
730 Quaas, J. (2021). An underestimated negative cloud feedback from cloud lifetime changes. *Nature Climate*
731 *Change*, *11*(6), 508–513. https://doi.org/10.1038/s41558-021-01038-1
732 Myers, T. A., Scott, R. C., Zelinka, M. D., Klein, S. A., Norris, J. R., & Caldwell, P. M. (2021). Observational
733 constraints on low cloud feedback reduce uncertainty of climate sensitivity. *Nature Climate Change*, *11*(6),
734 501–507. https://doi.org/10.1038/s41558-021-01039-0
735 Neubauer, D., Ferrachat, S., Siegenthaler-Le Drian, C., Stier, P., Partridge, D. G., Tegen, I., Bey, I., Stanelle, T.,
736 Kokkola, H., & Lohmann, U. (2019). The global aerosol–climate model ECHAM6.3–HAM2.3 – Part 2:
737 Cloud evaluation, aerosol radiative forcing, and climate sensitivity. *Geoscientific Model Development*,
738 *12*(8), 3609–3639. https://doi.org/10.5194/gmd-12-3609-2019
739 Qin, Y., Zelinka, M. D., & Klein, S. A. (2022). On the Correspondence Between Atmosphere-Only and Coupled
740 Simulations for Radiative Feedbacks and Forcing From CO_2. *Journal of Geophysical Research:*
741 *Atmospheres*, *127*(3). https://doi.org/10.1029/2021JD035460
742 Qu, X., Hall, A., Klein, S. A., & Caldwell, P. M. (2015). The strength of the tropical inversion and its response to
743 climate change in 18 CMIP5 models. *Climate Dynamics*, *45*(1), 375–396. https://doi.org/10.1007/s00382-
744 014-2441-9
745 Radtke, J., Mauritsen, T., & Hohenegger, C. (2021). Shallow cumulus cloud feedback in large eddy simulations –
746 bridging the gap to storm-resolving models. *Atmospheric Chemistry and Physics*, *21*(5), 3275–3288.
747 https://doi.org/10.5194/acp-21-3275-2021
748 Redelsperger, J.-L., Guichard, F., & Mondon, S. (2000). A Parameterization of Mesoscale Enhancement of Surface
749 Fluxes for Large-Scale Models. *Journal of Climate*, *13*(2), 402–421. https://doi.org/10.1175/1520-
750 0442(2000)013<0402:APOMEO>2.0.CO;2

751 Richter, J. H., Chen, C., Tang, Q., Xie, S., & Rasch, P. J. (2019). Improved Simulation of the QBO in E3SMv1.
752 *Journal of Advances in Modeling Earth Systems*, *11*(11), 3403–3418.
753 https://doi.org/10.1029/2019MS001763
754 Ringer, M. A., Andrews, T., & Webb, M. J. (2014). Global-mean radiative feedbacks and forcing in atmosphere-
755 only and coupled atmosphere-ocean climate change experiments. *Geophysical Research Letters*, *41*(11),
756 4035–4042. https://doi.org/10.1002/2014GL060347
757 Salzmann, M., Ferrachat, S., Tully, C., Münch, S., Watson-Parris, D., Neubauer, D., Siegenthaler-Le Drian, C., Rast,
758 S., Heinold, B., Crueger, T., Brokopf, R., Mülmenstädt, J., Quaas, J., Wan, H., Zhang, K., Lohmann, U.,
759 Stier, P., & Tegen, I. (2022). The Global Atmosphere-aerosol Model ICON-A-HAM2.3–Initial Model
760 Evaluation and Effects of Radiation Balance Tuning on Aerosol Optical Thickness. *Journal of Advances in*
761 *Modeling Earth Systems*, *14*(4). https://doi.org/10.1029/2021MS002699
762 Shell, K. M., Kiehl, J. T., & Shields, C. A. (2008). Using the Radiative Kernel Technique to Calculate Climate
763 Feedbacks in NCAR's Community Atmospheric Model. *Journal of Climate*, *21*(10), 2269–2282.
764 https://doi.org/10.1175/2007JCLI2044.1
765 Sherwood, S. C., Bony, S., & Dufresne, J.-L. (2014). Spread in model climate sensitivity traced to atmospheric
766 convective mixing. *Nature*, *505*(7481), Article 7481. https://doi.org/10.1038/nature12829
767 Soden, B. J., Held, I. M., Colman, R., Shell, K. M., Kiehl, J. T., & Shields, C. A. (2008). Quantifying Climate
768 Feedbacks Using Radiative Kernels. *Journal of Climate*, *21*(14), 3504–3520.
769 https://doi.org/10.1175/2007JCLI2110.1
770 Vial, J., Bony, S., Stevens, B., & Vogel, R. (2017). Mechanisms and Model Diversity of Trade-Wind Shallow
771 Cumulus Cloud Feedbacks: A Review. *Surveys in Geophysics*, *38*(6), 1331–1353.
772 https://doi.org/10.1007/s10712-017-9418-2
773 Vogel, R., Albright, A. L., Vial, J., George, G., Stevens, B., & Bony, S. (2022). Strong cloud–circulation coupling
774 explains weak trade cumulus feedback. *Nature*, *612*(7941), Article 7941. https://doi.org/10.1038/s41586-
775 022-05364-y
776 Vogel, R., Nuijens, L., & Stevens, B. (2016). The role of precipitation and spatial organization in the response of
777 trade-wind clouds to warming. *Journal of Advances in Modeling Earth Systems*, *8*(2), 843–862.
778 https://doi.org/10.1002/2015MS000568

779 Wang, Y.-C., Pan, H.-L., & Hsu, H.-H. (2015). Impacts of the triggering function of cumulus parameterization on
780 warm-season diurnal rainfall cycles at the Atmospheric Radiation Measurement Southern Great Plains site:
781 CONVECTIVE TRIGGER ON SGP NOCTURNAL RAIN. *Journal of Geophysical Research:*
782 *Atmospheres*, *120*(20), 10,681-10,702. https://doi.org/10.1002/2015JD023337
783 Webb, M. J., Senior, C. A., Sexton, D. M. H., Ingram, W. J., Williams, K. D., Ringer, M. A., McAvaney, B. J.,
784 Colman, R., Soden, B. J., Gudgel, R., Knutson, T., Emori, S., Ogura, T., Tsushima, Y., Andronova, N., Li,
785 B., Musat, I., Bony, S., & Taylor, K. E. (2006). On the contribution of local feedback mechanisms to the
786 range of climate sensitivity in two GCM ensembles. *Climate Dynamics*, *27*(1), 17–38.
787 https://doi.org/10.1007/s00382-006-0111-2
788 Xie, S., Wang, Y., Lin, W., Ma, H., Tang, Q., Tang, S., Zheng, X., Golaz, J., Zhang, G. J., & Zhang, M. (2019).
789 Improved Diurnal Cycle of Precipitation in E3SM With a Revised Convective Triggering Function.
790 *Journal of Advances in Modeling Earth Systems*, *11*(7), 2290–2310.
791 https://doi.org/10.1029/2019MS001702
792 Xie, S., & Zhang, M. (2000). Impact of the convection triggering function on single-column model simulations.
793 *Journal of Geophysical Research: Atmospheres*, *105*(D11), 14983–14996.
794 https://doi.org/10.1029/2000JD900170
795 Zelinka, M. (2022). *mzelinka/cmip56_forcing_feedback_ecs: Jun 15, 2022 Release* (v2.2). Zenodo.
796 https://doi.org/10.5281/ZENODO.6647291
797 Zelinka, M. D., Klein, S. A., & Hartmann, D. L. (2012). Computing and Partitioning Cloud Feedbacks Using Cloud
798 Property Histograms. Part I: Cloud Radiative Kernels. *Journal of Climate*, *25*(11), 3715–3735.
799 https://doi.org/10.1175/JCLI-D-11-00248.1
800 Zelinka, M. D., Klein, S. A., Qin, Y., & Myers, T. A. (2022). Evaluating Climate Models' Cloud Feedbacks Against
801 Expert Judgment. *Journal of Geophysical Research: Atmospheres*, *127*(2).
802 https://doi.org/10.1029/2021JD035198
803 Zelinka, M. D., Myers, T. A., McCoy, D. T., Po-Chedley, S., Caldwell, P. M., Ceppi, P., Klein, S. A., & Taylor, K.
804 E. (2020). Causes of Higher Climate Sensitivity in CMIP6 Models. *Geophysical Research Letters*, *47*(1).
805 https://doi.org/10.1029/2019GL085782

806 Zelinka, M. D., Zhou, C., & Klein, S. A. (2016). Insights from a refined decomposition of cloud feedbacks.
807 *Geophysical Research Letters*, *43*(17), 9259–9269. https://doi.org/10.1002/2016GL069917
808 Zhang, G. J., & McFarlane, N. A. (1995). Sensitivity of climate simulations to the parameterization of cumulus
809 convection in the Canadian climate centre general circulation model. *Atmosphere-Ocean*, *33*(3), 407–446.
810 https://doi.org/10.1080/07055900.1995.9649539
811 Zhang, H., Wang, M., Guo, Z., Zhou, C., Zhou, T., Qian, Y., Larson, V. E., Ghan, S., Ovchinnikov, M.,
812 Bogenschutz, P. A., & Gettelman, A. (2018). Low-Cloud Feedback in CAM5-CLUBB: Physical
813 Mechanisms and Parameter Sensitivity Analysis. *Journal of Advances in Modeling Earth Systems*, *10*(11),
814 2844–2864. https://doi.org/10.1029/2018MS001423
815